1   Metal deportment in Pb-Zn mine wastes from a historic tailings pond, Plombières, East Belgium

2   Srećko Bevandić[1], Rosie Blannin[2], Alexandra Gomez Escobar[3], Kai Bachmann[2], Max Frenzel[2], Álvaro
3   Pinto[3], Jorge M. R. S. Relvas[3] and Philippe Muchez[1]

4   [1] KU Leuven, Department of Earth and Environmental Sciences, Celestijnenlaan 200E, B-3001 Leuven,
5   Belgium

6   [2] Helmholtz-Zentrum Dresden-Rossendorf, Helmholtz Institute Freiberg for Resource Technology,
7   Chemnitzer Strasse 40, 09599 Freiberg, Germany

8   [3] Instituto Dom Luiz, Faculdade de Ciências, Universidade de Lisboa, 1749-016 Lisbon, Portugal

9   Abstract:

10   The exploitation of mine waste materials as secondary resources requires in-depth mineralogical analyses,
11   with metal deportment being of particular relevance for metal recovery. Using a combination of the
12   Scanning Electron Microscope (SEM)-based Mineral Liberation Analyser (MLA) and Electron Probe Micro-
13   Analyser (EPMA) methods, the deportment of lead and zinc in the historic Plombières mine site (East
14   Belgium) was investigated. The mine site comprises four different materials: soil, metallurgical waste,
15   brown and yellow tailings. The integration of the MLA and EPMA data allowed the identification and
16   quantification of Pb- and Zn-bearing phases, including minerals present in low abundances as well as slag
17   phases. Different slag types and Pb oxides phases are the main sources of lead in Plombières mine waste
18   samples. These phases host 65 to 99 % of the Pb, the rest is distributed between cerussite (0 to 37 %),
19   and/or anglesite (0 to 17 %). Approximately 95 % of Zn is hosted by different types of slags or by
20   fraipontite, with minor amounts contributed by sphalerite (0.1 to 3 %), gahnite (1.0 to 2.4 %), willemite
21   (0.1 to 2.9 %), and bannisterite (0 to 3 %). The MLA/EPMA measurements were validated by comparing
22   calculated Pb and Zn grades with bulk grades measured by X-ray fluorescence spectroscopy. The
23   coefficients of correlation between the measured and calculated values were found to be 0.89 for lead
24   and 0.80 for zinc. Uncertainties on the metal deportments were estimated by bootstrap resampling and
25   are typically low. The highest uncertainties are observed when the metal-bearing phases are present in
26   low abundances, which is particularly noticeable in the yellow tailings. Considering the promising results,
27   the integrated approach applied in this study should be applicable to other metals and waste deposits
28   across the globe.

29   Keywords: Elemental deportment, mine waste, automated mineralogy, nugget effect

1. Introduction

The extraction and processing of ore result in large amounts of mine waste materials, including tailings, metallurgical wastes and waste rock (Lottermoser., 2011; Tayebi-Khorami et al., 2019). Mine waste materials can potentially present economic prospects for re-use and re-mining, but can also cause severe damage and contamination to the environment if stored improperly (Jamieson et al., 2015; Ettler, 2015; Falagán et al., 2017; Karaca et al., 2017; Ceniceros-Gómez et al., 2018; Helser and Cappuyns, 2021; Amar et al., 2021). Sulphidic mine waste materials have the potential to produce Acid Rock Drainage (ARD) and leach toxic elements into the environment when exposed to oxidising conditions, with negative effects on the environment and human health (Environment Agency, 2009). Therefore, the re-use of mine waste materials can also be beneficial for the mitigation of environmental risks.

Sulphide ores are important sources for metals of economical interest, metals such as zinc, lead, copper, and nickel (Lottermoser, 2011; Lindsay et al., 2015;), which are hosted by the ore minerals sphalerite (ZnS), galena (PbS), chalcopyrite ($CuFeS_2$) and pentlandite [$(Fe, Ni)_9S_8$], respectively. Mining waste typically comprises gangue minerals and low contents of the ore minerals which were not recovered during processing. Historic mine wastes tend to contain higher amounts of ore minerals than modern mine wastes, in direct relation to the lower processing efficiency, as well as exploitation of higher grade ores, in the past (Martinez et al., 2016; Hudson-Edwards et al., 2011). Moreover, many elements whose extraction was previously not economically feasible to mine are now desirable and vital for high-tech applications, e.g. cobalt, indium, germanium, and gallium (Dold, 2020). Therefore, it may also be economically viable to re-process mining wastes to recover the remaining quantities of such metals.

Low-grade deposits such as mining waste require efficient extraction processes for metal recovery to be economically feasible (Hesse et al., 2017). Recent studies have shown that in-depth mineralogical and geochemical analyses, together with textural information, are required to optimise processing parameters and improve metal recovery (Guanira et al., 2020). The application of these methods to both ores and mine wastes enables the economic potential of ore deposits to be maximised, which would in turn decrease the risks of the corresponding financial investments. Furthermore, knowledge of the chemistry and mineralogy of the materials is also beneficial for environmental assessments (Parbhakar-Fox et al., 2011; Gomez-Arias et al., 2021). For example, in-depth analysis of tailings can help with the prediction of ARD (acid rock drainage) potential. These kinds of analyses could be incorporated during the early stages of a mining operation and may lead to the easier obtainment of environmental licences (Parbhakar-Fox et al., 2018).

Elemental deportment is one of the most important factors to consider during the characterisation of an ore for processing (Frenzel et al., 2019). Deportment studies have been accomplished for platinum group elements (PGEs), rare earth elements (REEs), gold, silver, copper, iron, chromium, indium and germanium in different ore types (Gregory et al., 2013; Elghali et al., 2018; Frenzel et al., 201; Polko et al., 2019; Schulz et al., 2019; Tripathy et al., 2019). The most precise results are achieved by combining several different analytical methods. Appropriate methods may include X-ray diffraction (XRD), X-ray fluorescence (XRF), inductively coupled plasma atomic emission spectroscopy (ICP-OES), and electron probe micro-analyser (EPMA). Scanning electron microscope (SEM)-based automated mineralogical methods (e.g. MLA, QEMSCAN, TIMA) have been proven to be an efficient way to characterise textural and mineralogical ore properties which are relevant for the extraction of the metals (Kern et al., 2018; Guanira et al., 2020; Schulz et al., 2020; Pereira et al., 2021a; Pereira et al., 2021b). Chemical methods such as XRF and ICP-

72 OES are equally important for deportment calculations since they are used to assess the quality and
73 reliability of the Mineral liberation analyser (MLA) measurements and deportment calculations (Kern et
74 al., 2018; Frenzel et al., 2019; Blannin et al., 2021; Swinkels et al., 2021).

75 Based on a search at "Web of science" using the words "deportment"; "mine waste" or "tailings" more
76 than 20 publications appeared, however by adding terms "slags and/ or non-minerals" only one
77 publication of by Tuhy et al. (2020) matched these criteria (last checked 11/01/2022). Tuhy et al. (2020)
78 focused on quantitatively determining the contaminant partitioning in the topsoil by integrating
79 automated mineralogy (autoSEM) with standard mineralogical techniques (XRD, SEM/EDS, EPMA). Up to
80 date, this is the only other study that used automated techniques to establish mineral deportment from
81 mine waste that consists of minerals and slags. Most of the studies found using terms "deportment" and
82 "mine waste or tailings" rely on bulk mineralogical and geochemical analyses to assess the economic
83 potential and environmental issues (e.g. Titshall et al., 2013; Cabala et al., 2019; Kuhn and Meima, 2019).
84 Some studies have investigated lead and/or zinc deposits, but the focus is most often on precious or
85 penalty elements (e.g. Ag, Ga, Ge, In, Sb, Cd) (Minz et al., 2015; Mondillo et al., 2018; Mikulski et al.,
86 2020). This is the first study to deal with the detailed characterisation of the lead and zinc deportment of
87 materials from the Plombières tailings pond. The specific complexity of these materials lies in their mixed
88 nature, comprising residues from both the physical and pyrometallurgical processing of the ores.

89 The Plombières tailings pond in East Belgium covers a minimum surface area of 8000 m^2 and is composed
90 of 4 types of material: soil, metallurgical waste, brown and yellow tailings (Bevandić et al., 2021). The mine
91 waste material represents residues of the pyrometallurgical processing of Mississippi Valley-type (MVT)
92 ores (Dejonghe et al., 1993; Kucha et al., 1996). The primary mineralogy of the Plombières ore consisted
93 mostly of the sulfide minerals galena (PbS), sphalerite (ZnS) and pyrite/marcasite (FeS_2), with gangue
94 minerals including quartz and carbonates (Dejonghe et al., 1998; Baele et al., 2021). Bulk geochemical
95 analysis (XRF) showed that the different types of mine waste material dominantly consist of SiO_2, Al_2O_3
96 and Fe_2O_3, while the lead and zinc contents vary from 51 ppm to 24 wt % and from 10 ppm to 10.1 wt %,
97 respectively (Bevandić et al., 2021). Bulk mineralogical analyses (XRD) corroborated these findings,
98 demonstrating that the major minerals present are quartz, amorphous phases (most likely
99 pyrometallurgical slags) and phyllosilicates, with minor amounts of Fe-, Pb- and Zn-bearing minerals
100 (Bevandić et al., 2021). The metallurgical waste layer of the mine wastes was found to have a similar
101 composition to nearby metallurgical dumps that were characterised by Kucha et al., (1996).

102 Although bulk mineralogical analytical methods can provide information on the presence of minor to
103 major minerals, difficulties may occur with trace minerals (Warlo et al., 2019). Therefore, these methods
104 may not be ideal for low-grade materials such as mine wastes. For example, when using XRD to
105 characterise the bulk mineralogy of the different material types of the Plombières tailings pond, Bevandić
106 et al. (2021) encountered problems due to the nature of the mine waste materials. Quantification of XRD
107 results was complicated by the presence of amorphous phases, with broad and low-intensity peaks
108 covering the peaks of mineral phases present in low-quantities (Bevandić et al., 2021). In particular, Pb-
109 and Zn-bearing minerals, which occur in low abundances, could not be identified (Bevandić et al., 2021).
110 Additionally, lead and zinc are likely to occur in the amorphous phases (Kucha et al., 1996). The
111 contribution of these materials to the overall lead and zinc deportment could not be assessed with XRD,
112 meaning that the deportments calculated from solely the XRD results would be incorrect.

113 This study aimed to determine the elemental distribution of lead and zinc within the different mine waste
114 materials present in the Plombières mine waste (East Belgium) by analysing selected samples with a
115 combination of MLA and EPMA. Several studies have shown that the integration of these methods can
116 efficiently resolve relevant mineral and slag phases, and provide accurate estimates of their contributions
117 to the metal deportment (Rao and Das et al., 2014; Wang et al., 2015; Horckmans et al., 2019; Morrison
118 et al., 2019; Gomez-Arias et al., 2022). The benefits of metal deportment studies for mine waste materials
119 were assessed, with a particular focus on the characterisation of non-crystalline slag phases, which was
120 not achieved in previous studies. The procedures used in this study can be applied to other mine wasted
121 deposits around the globe, to lead to the optimisation of suitable processing routes.

122 2. Material and methodology

123 2.1. Sampling and sample preparation

124 More than 120 samples were collected from 20 drill holes extracted during a sampling campaign of the
125 Plombières tailings pond (Bevandić et al., 2021). Twenty-three of these samples were selected for this
126 study to cover the variability in mineralogy, lead and zinc contents, as determined in the previous study
127 (Bevandić et al., 2021). The brown and yellow tailings have lower contents of the metals of interest, and
128 no lead and/or zinc phases were detected with XRD in these materials (Bevandić et al. 2021). Therefore,
129 to ensure that a sufficient number of lead and zinc grains would be detected in all of the four types of
130 mine wastes, additional samples of brown and yellow tailings were selected for MLA and EPMA analyses.
131 Before further analysis, samples were dried, deagglomerated and split using a riffle splitter. Subsamples
132 were prepared using the incremental sampling methodology (ISM). One increment was used for the
133 preparation of grain mounts for MLA and EPMA. After enough material was taken for the grain mount
134 preparation, the remainder of the increment was used for X-ray fluorescence (XRF) analysis at an external
135 laboratory. An overview of the analytical methods used on different types of mine waste samples for in-
136 depth analysis is provided in Electronic Supplementary Material 1 (Table A1 in ESM1). The bulk
137 geochemical analyses using the XRF method were conducted at the ACME laboratory in Canada. Details
138 are provided in ESM2. The steps of sample preparation undertaken for this study are outlined in the
139 following subsections.

140 2.2. Mineral liberation analyser (MLA)

141 Quantitative mineralogical analysis using MLA was carried out on 23 samples (4 of soil, 5 of metallurgical
142 waste, 6 of brown tailings and 8 of yellow tailings) (Table A1). Polished grain mounts (30 mm diameter)
143 were prepared at the Helmholtz Institute Freiberg (HIF) for Resource Technology, by mixing the samples
144 with graphite powder and epoxy resin. In order to mitigate the effects of gravity settling, each epoxy block
145 was sliced into 5 strips, which were then rotated by 90°, re-embedded in epoxy resin and polished (Heinig
146 et al., 2015). After carbon-coating of the samples, measurements were performed at the HIF on an FEI
147 Quanta 650F field emission scanning electron microscope equipped with two Bruker Quantax X-flash 5030
148 energy-dispersive X-rays (EDX) detectors and the MLA software (version 3.15). The GXMAP mode was
149 applied with an acceleration voltage of 15 kV, image resolution of 1 μm/pixel, step size of 6 pixels, and
150 BSE brightness calibrated to Au (Fandrich et al., 2007; Bachmann et al., 2017). The machine settings and
151 other measurements parameters used are given in Table A2 in ESM1

152 Measurement conditions and sample preparations for the MLA were determined by the type of material.
153 Both types of tailings were measured and prepared under the same conditions, while the sample
154 preparation used for the soil and metallurgical waste samples were different. The main reasons for this

155 were the fine-grained nature of tailings in comparison to the metallurgical waste and soil, and the
156 presence of coal in the metallurgical waste and soil. The presence of carbon phases requires measurement
157 conditions suitable for distinguishing these phases from the graphite powder introduced during sample
158 preparation since they have similar Back Scatter Electron (BSE) values. Detailed information about
159 methods suitable for measuring and processing samples with organic matter such as coal can be found in
160 the work done by Rahfeld and Gutzmer (2017). Recently, the efficiency of this study was confirmed with
161 research on lithium-ion batteries that consist both of mineral, non-mineral and carbon particles
162 (Vanderbruggen et al., 2021).

163 Minerals were classified based on their EDX spectra. Slag particles could be clearly distinguished from
164 other particles with the SEM by their morphology and texture. Since the MLA software does not classify
165 particles based on these visual criteria, this was done manually. Therefore, EDX spectra of these phases
166 were collected and used to quantify their chemical compositions. Based on the collected spectra, different
167 types of slags were defined. The characterisation of the slags was difficult due to their compositional
168 heterogeneity, and therefore, several EDX spectra were collected for each type to aid classification. The
169 threshold for spectral matching was set at 95 % for GXMAP measurements. Processing of the MLA data
170 was performed until the content of unknown phases was less than 0.5 wt. %.

171 2.3. Electron probe micro-analyser (EPMA)
172 EPMA analyses were carried out on 11 samples to more accurately quantify the chemical composition of
173 the various Pb- and Zn-bearing phases. Samples for EPMA were selected based on the mineralogy
174 obtained by MLA analysis. Three samples of each material type were selected, except for the yellow
175 tailings, for which two samples were selected. Prior to analysis, the diameter of the grain mounts was
176 reduced from 30 mm to 25 mm, and the surface was re-polished. Reflective light microscopy was
177 performed on a Leica microscope, equipped with a halogen lamp, to identify minerals and areas of interest
178 for EPMA measurements.

179 Microprobe analysis was performed at the Instituto Dom Luiz, Faculdade de Ciências, University of Lisbon,
180 Lisbon, Portugal. The analysis was performed with a JEOL JXA 8200 electron microprobe equipped with
181 four tunable wavelength dispersive spectrometers (WDS) and one energy dispersive X-Ray spectrometer
182 (EDX). The machine settings and other measurements parameters used are described in Table A3 in ESM1.
183 Approximately 800 point analyses and 20 compositional maps were made. Slag grains in particular were
184 targeted for point analyses to better capture the strong compositional heterogeneity of these phases.
185 Since they represent a significant proportion of the mine waste material, it was vital to precisely establish
186 their chemical composition for the deportment calculations. In total, 400 points from different slag grains
187 were measured. Around 160 point analyses of Pb-bearing minerals and 25 of Zn-bearing minerals were
188 measured. Additionally, EPMA analysis was used to identify Pb oxide grains to avoid the overlapping of
189 Pb-S peaks in EDX. The lower number of measured points for the Zn-bearing minerals is due to the majority
190 of the Zn-bearing mineral grains being too fine to obtain accurate measurements with EPMA (Figure A1
191 in ESM 1). In addition, grains of pyrite and calcite were measured with EPMA, since they may sometimes
192 contain elevated Zn contents (Liu et al., 2018; Zhang et al., 2020). The collected data were combined with
193 the MLA results to improve the quality of the overall results and develop a quantitative deportment
194 model, as described in the following section. Point analyses collected for this study can be found in the
195 ESM3.

196   2.4. Deportment calculation

197   In order to obtain quantitative metal deportments, the MLA and EPMA data need to be integrated. Firstly,
198   the bulk concentration (Ck) of the metal of interest (k) in the sample was calculated with Eq. 1 (Frenzel et
199   al., 2019). Since the bulk concentration calculations are the basis of the deportment study, it is of the
200   highest importance to have reliable phase abundances (xi) and elemental chemistry (ci) of the phases of
201   interest. Quantitative results of modal abundance (xi) are obtained from MLA measurements and
202   quantitative results of element chemistry (ci) are obtained from EPMA point analysis.

$$C_k = \sum_{i=1}^{N} c_i * x_i$$

203

204   Eq. 1. After Frenzel et al. (2019), with N the number of phases in the sample.

205   Mineralogical deportments (Md$_k$) were subsequently calculated with Eq. 2 (cf. Frenzel et al., 2019) for
206   each individual phase that contributes to the bulk concentration of a specific metal of interest.

$$Md_k = \left\{ \frac{c_i * x_i}{C_k} * 100\ \% \right\}_{i=1,\dots,N}$$

207

208   Eq. 2 After Frenzel et al. (2019)

209   Up to date, some studies dealing with the characterisation of mine waste material (e.g. tailings) are using
210   mineralogical reconciliation methods to validate bulk geochemical data (e.g. Elghali et al., 2018; Elghali
211   et al., 2021). The latter method consists of changing quantified mineralogy data collected by automated
212   mineralogical methods (e.g. QEMSCAN) to fit measured geochemical data. However, given the complex
213   nature of the Plombières mine waste materials, including different types of slag material with varying
214   composition (Bevandić et al., 2021), there is no way of unambiguously adjusting the mineralogical data
215   using the chemical assays. Making assumptions, e.g. considering the elemental chemistry of the slagas
216   constant would result in not considering the uncertainties present and would introduce bias into the
217   deportment calculations. Based on recent studies (e.g. Kern et al., 2018; Frenzel et al., 2019; Blannin et
218   al., 2021; Swinkels et al., 2021) the methodology of deportment model validation with bulk chemistry, as
219   carried out in the present study is considered as a more suitable option for Plombières mine waste.
220   Therefore, taking into account the quality and reliability of MLA/EPMA measurements, calculated lead
221   and zinc grades (including a calculated 95 % confidence interval) were compared to the contents
222   measured by bulk analysis with XRF. Moreover, by doing calculation and validation of the data as
223   suggested, the authors are showing how mineralogical (xi) and mineral/slag elemental chemistry (ci)
224   uncertainties translate into deportment and chemical assay uncertainties, which has not been done until
225   now.

226   2.5. Bootstrap resampling

227   Bootstrap resampling is a technique that has proven to be effective for the estimation of analytical
228   uncertainties on automated SEM-based image analysis data (Napier-Munn, 2013; Mariano and Evans,
229   2015; Frenzel et al., 2019; Blannin et al., 2021). This technique is applicable to modal mineralogy, grain
230   size distribution, mineral association, deportment calculations, and other results that can be obtained
231   from automated SEM-based image analysis (Evans and Napier-Munn, 2013; Mariano and Evans, 2015;
232   Blannin et al. 2021).

233 In order to perform bootstrap resampling, the original sample is divided into representative subsamples.
234 To assess the extent of analytical uncertainties, individual sub-samples are randomly selected and
235 combined with others to create potential realisations of the original sample (Evans and Napier-Munn,
236 2013; Mariano and Evans, 2015; Blannin et al., 2021). The spread in the reconstructed properties of these
237 realisations provides a reasonable estimate of the measurement uncertainties. Before calculation of the
238 deportment, it was important to establish the uncertainty on all previously acquired data, to understand
239 how these uncertainties are translated to the deportment calculation (Frenzel et al., 2019).

240 In this study, the original grain mount was cut into 5 strips, as previously mentioned. Each strip was taken
241 as a representative sub-sample. Bootstrap resampling was performed on the classified and processed MLA
242 data, with 1000 simulations for each sample. For this study, the uncertainties of the modal mineralogy,
243 abundance and composition of Pb- and Zn-bearing phases were estimated, as well as the bulk
244 concentrations calculated from the integration of the MLA and EPMA data.

3. Results

246 The following subsections present the analytical results by combining MLA and EPMA. The modal
247 mineralogy, slag characterisation and the lead and zinc deportment are presented. Additionally, the
248 uncertainties related to the MLA measurements are assessed, together with calculations of deportment
249 and bulk concentration.

3.1. Modal mineralogy

251 In total, 47 mineral phases and 4 types of pyrometallurgical slags were identified in the samples using MLA
252 and EPMA. For simplification, 10 groupings were applied to these 51 phases, as summarized in Table A4
253 in ESM1. The groups of interest for this study are slags, and Pb- and Zn- bearing minerals, which will be
254 discussed in detail in the following sections.

255 The MLA results show that all 4 material types predominantly consist of quartz (SiO_2), phyllosilicate and
256 slag phases. These three phases alone comprise more than 80 wt. % of the material in each mine waste
257 type (Figure 1 and Table A5 in ESM1). Quartz varies in content from 3 - 57 wt. %, phyllosilicates 2 - 35 wt.
258 % and slags 6 - 59 wt. %. As the quartz content increases, the content of slags tends to decrease. Other
259 minerals (e.g. apatite, barite, zircon) are usually minor or trace constituents (Figure 1). The modal
260 mineralogies of the different mine waste materials are plotted in Figure 1. It is apparent that the soil and
261 metallurgical waste samples have similar compositions, in particular, a high ratio of slags to minerals when
262 compared to the tailing samples. These two types of material are distinguished by the higher content of
263 Zn-bearing minerals in the metallurgical waste and the presence of coal in the soils. In both types of
264 tailings, slags are present as a minor constituent. Quartz is most abundant in tailings, while in the soil and
265 metallurgical waste it is present as a minor constituent. Pb-bearing minerals are most abundant in the
266 brown tailing samples, while Zn-bearing minerals are most abundant in the metallurgical waste samples
267 The median modal mineralogy of all studied samples can be found in Table A5 in ESM1.

268 To assess the uncertainties of the modal mineralogy measurements, the median modal abundances for
269 different phases were plotted with error bars representing the 2.5[th] and 97.5[th] percentiles. Uncertainties
270 for all samples are shown in Figure A2 in ESM 1. Quartz, phyllosilicates, feldspars and slags typically have
271 relative standard deviations (RSD) of less than 10 %, but mostly less than 5 %, in all 4 types of material.
272 Iron, titanium, lead and zinc minerals, coal and carbonates tend to have higher and more variable RSDs (2
273 to 30 %), depending on their content in the sample. As could be expected, phases with low modal

274 abundances have higher RSD (e.g., Blannin et al., 2021). The RSD of the contents of the Pb- and Zn-bearing
275 phases will be presented in the following sections.
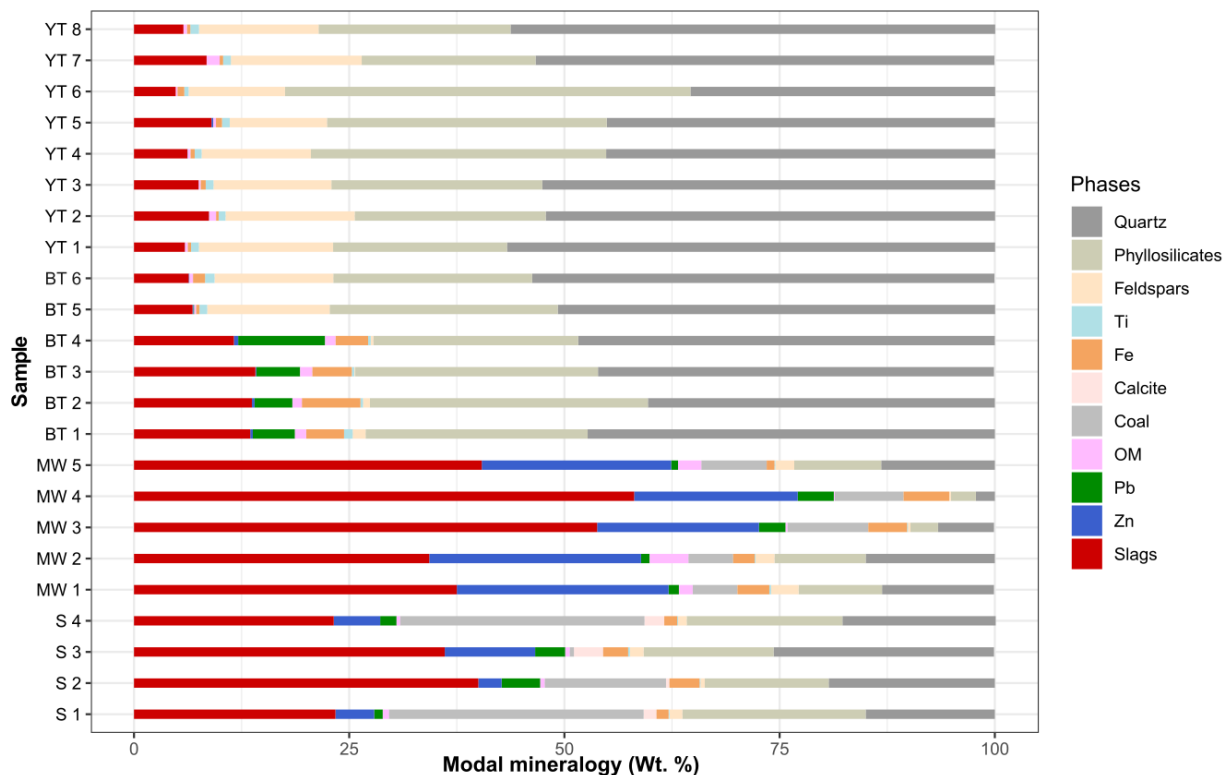
276

277 Figure 1. Median modal mineralogy values of studied mine waste samples, from bootstrap resampling of
278 the MLA results. S – soil; MW – metallurgical waste; BT – brown tailings; YT – yellow tailings.; Ti – Ti
279 minerals; Fe – Fe minerals; OM – other minerals; Pb – Pb minerals; Zn – Zn minerals.

280 3.2. Slag characterisation
281 The different slag phases were characterised by MLA and EPMA. Slags are aggregates of synthetically
282 produced phases, formed during pyrometallurgical processing of the ore, that often show a high degree
283 of compositional heterogeneity (e.g., Piatak et al., 2015). In the Plombières mine waste, four different
284 types of slag were identified. SiO_2-rich (SiS), SiO_2-Al_2O_3-rich (SAS), Fe_2O_3-rich (FS) and PbO-ZnO-rich (PZS)
285 slags. In Figure 2, all four types of slags are present in one particle. Many studies dealing with slags report
286 slags phases as mineral phases and assign them a mineral name based on their chemical composition
287 (Piatak et al., 2015). For the purposes of this study, and to avoid further complications of the already
288 complex material, the authors decided not to assign mineral names to the different slags phases.

289 Depending on the type of material, the abundances of the different slag types vary. In all soil samples, FS
290 (4 to 13 wt. %) and PZS (7 to 15 wt. %) phases are most abundant. For 3 out of the 5 metallurgical waste
291 samples, SiS (8 to 20 wt. %) and SAS (12 to 18 wt. %) types are most abundant, while the other 2 samples
292 of metallurgical waste are dominated by FS (~30 wt. %) and PZS (13 to 16 wt. %) slags. Brown tailings, on
293 average, contain similar amounts of SiS and PZS types of slag (~3-7 wt. %). In two samples (BT 5 and 6)
294 SAS (~ 4.7 wt. %) and SiS (~1.4 wt. %) are more abundant than FS and PZS slags. SiO_2-rich (SiS) (0.6 to 3.4
295 wt. %) and SAS (4.2 to 6.2 wt. %) slags are the most abundant slag types in the yellow tailings, while the

contents of the other types are < 0.1 wt. %. A full list of the slag types present in the measured samples can be found in Table A6 in ESM 1.
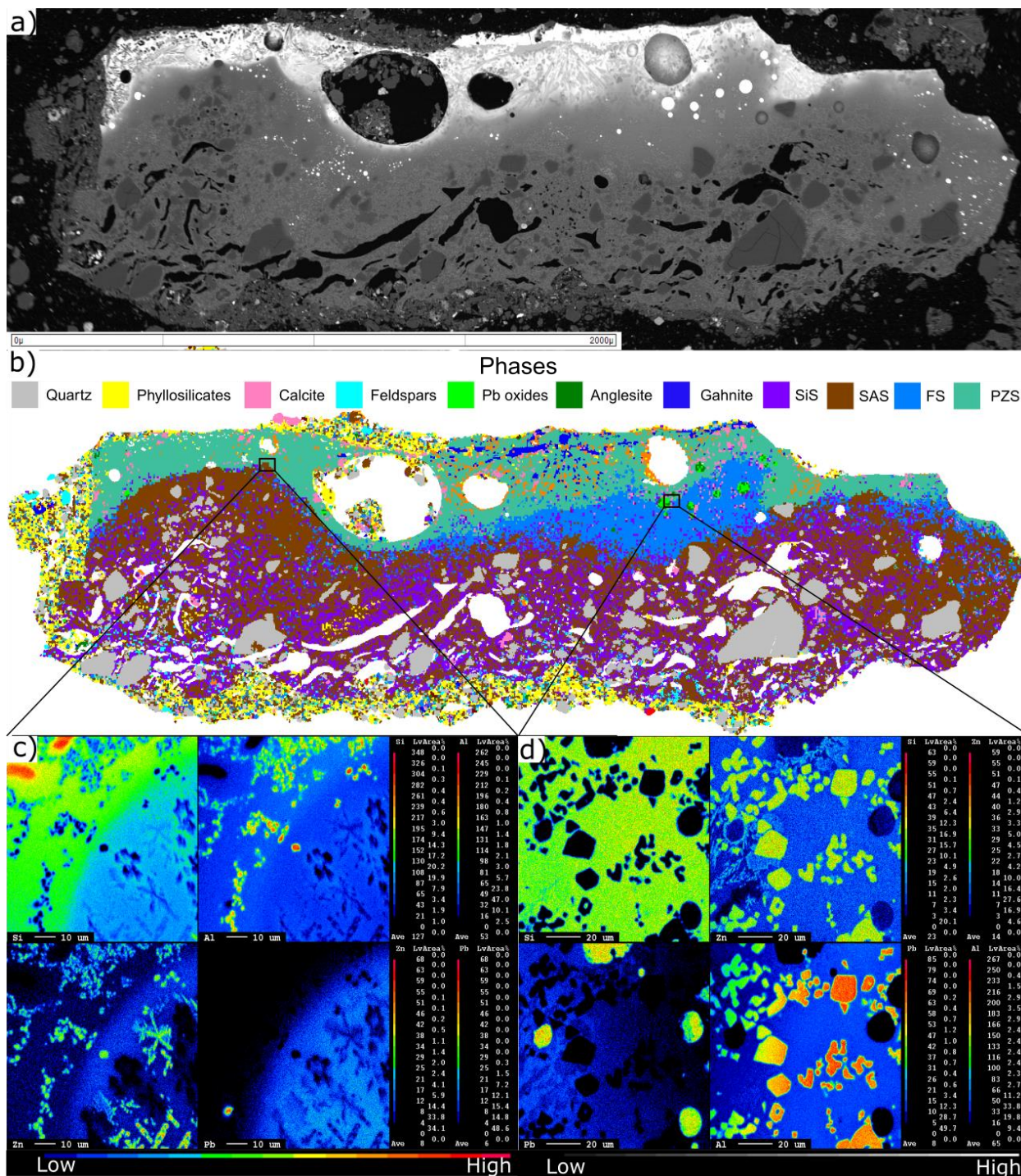
Figure 2. Backscattered electron (BSE) (a) and false coloured MLA (b) image of a slag particle. From the SEM-MLA image (b), it can be seen that the grains consist of quartz, 4 types of slag, phyllosilicates, Pb-oxide, anglesite, gahnite and other minerals. In the lower-left corner (c) the elemental maps of silicon, aluminium, lead and zinc show small-scale dendritic inclusions containing zinc and aluminium. These

303 inclusions were too small to be analysed with EMPA. On the right (d), the elemental maps show droplets
304 that mainly consist of Pb oxides. Additionally, larger grains of Zn-Al inclusions (gahnite) occur. SiS – SiO_2-
305 rich; SAS – SiO_2-Al_2O_3-rich; FS – Fe_2O_3-rich; PZS – PbO-ZnO-rich slags.

306 The composition of the SiO_2-rich slag is dominated by SiO_2 (average- 96.1 wt. %), with trace amounts of
307 Al_2O_3, Fe_2O_3, CaO, PbO and ZnO (Figure 3). The content of PbO and ZnO is minor ($\sim$ 0.1 wt. %). SAS slags
308 predominantly consist of SiO_2 (43.4 wt. %) and Al_2O_3 (17.3 wt. %), with minor amounts of Al_2O_3, Fe_2O_3,
309 CaO, PbO and ZnO (Figure 3). The major component of FS types of slags is iron (Fe_2O_3- 89.6 wt. %), with
310 minor amounts of lead (PbO- 3.1 wt. %), zinc (ZnO- 4.3 wt. %), aluminium (Al_2O_3- 3.1 wt. %) and silicon
311 (SiO_2- 7.7 wt. %) (Figure 3). Lead-zinc-rich slags consist of lead (PbO - 15. 8 wt. %) and zinc (ZnO- 37.0 wt.
312 %) (Figure 3). Other elements present in significant contents are silicon (SiO_2- 18.1 wt. %), aluminium
313 (Al_2O_3- 6.4 wt. %) and iron (Fe_2O_3- 8.7 wt. %) (Figure 3).
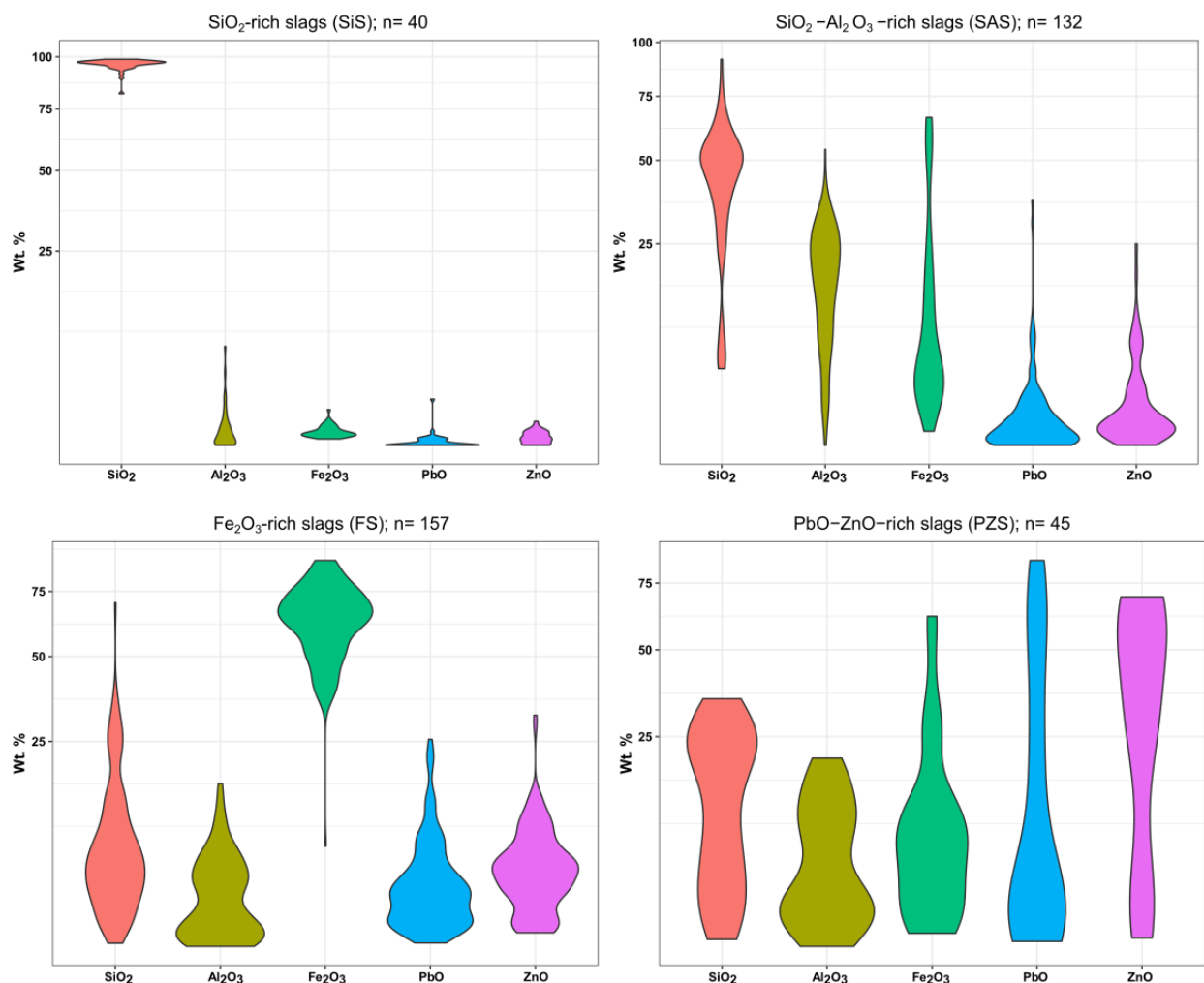
314

315 Figure 3. Chemical composition of major elements of 4 different types of slags.

316 3.3. Lead deportment
317 Several Pb-bearing minerals were identified with MLA and EPMA: Pb oxides (PbO/PbO_2), anglesite
318 ($PbSO_4$), cerussite ($PbCO_3$), plumbogummite ($PbAl_3(PO_4)_2(OH)_5 \cdot 5H_2O$) and Ca-bearing pyromorphite

319   ((Pb,Ca)$_5$(PO$_4$)$_3$Cl). In total, 161 point analyses were obtained for these minerals (Pb oxides n = 46,
320   anglesite, n = 72, cerussite n = 33, plumbogummite n = 5, and Ca-bearing pyromorphite n=5). The mineral
321   chemistry of the Pb-bearing minerals, as determined by EPMA, can be found in Table A7 in ESM 1.

322   EPMA revealed that the Pb oxide grains have a minor sulphur content (<0.2 wt. %). These grains contain
323   a core consisting of litharge (PbO), while the rim is more oxidised and closer to the chemical composition
324   of plattnerite (PbO$_2$) (cf. Figure 4). Furthermore, compositional mapping showed that grains identified as
325   plumbogummite by MLA partially consist of pyromorphite (Figure A3 in ESM 1).
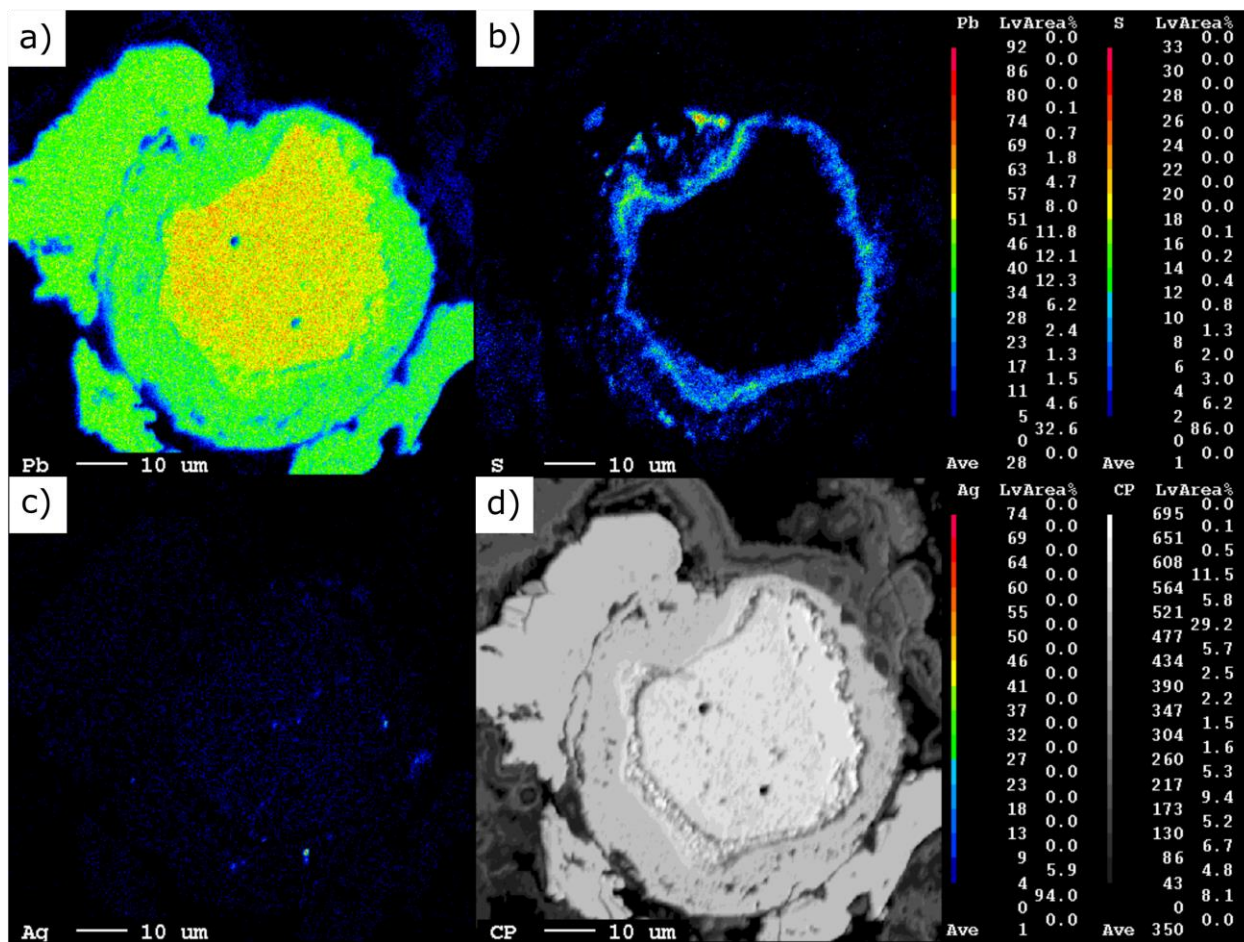
326

327   Figure 4. EPMA maps of Pb oxide grains, showing the distribution of lead (a), S (b) and Ag (c) and BSE
328   image (d)

329   The Pb-bearing minerals are most abundant in the brown tailings (4.4-10.0 wt. %), followed by soil (1.1-
330   4.6 wt. %), metallurgical waste (1.0-3.4 wt. %) and yellow tailings (<0.01 wt. %) (Figure 1 and Table A6 in
331   ESM 1). The most common Pb-bearing mineral in the metallurgical waste (1.1 - 2.9 wt. %), brown (3.5- 7.9
332   wt. %) and yellow (<0.01 wt. %) tailings is Pb oxide (Figure 5). In the metallurgical waste samples, cerussite
333   is the second-most abundant phase (0.1 - 0.5 wt. %), while in the brown tailings it is anglesite (0.8-1.8 wt.
334   %), followed by plumbogummite (0.1-0.5 wt. %) (Figure 5). In soil, anglesite (0.9-3.5 wt. %) is the most
335   common Pb-bearing mineral (Figure 5), followed by cerussite (0.1-0.8 wt. %), Pb oxides (0.1-0.3 wt. %)
336   and plumbogummite (<0.2 wt. %). However, the different types of slags still represent the highest content
337   of Pb-bearing phases in all 4 types of materials (Figure 5 and Table A6 in ESM 1).

338
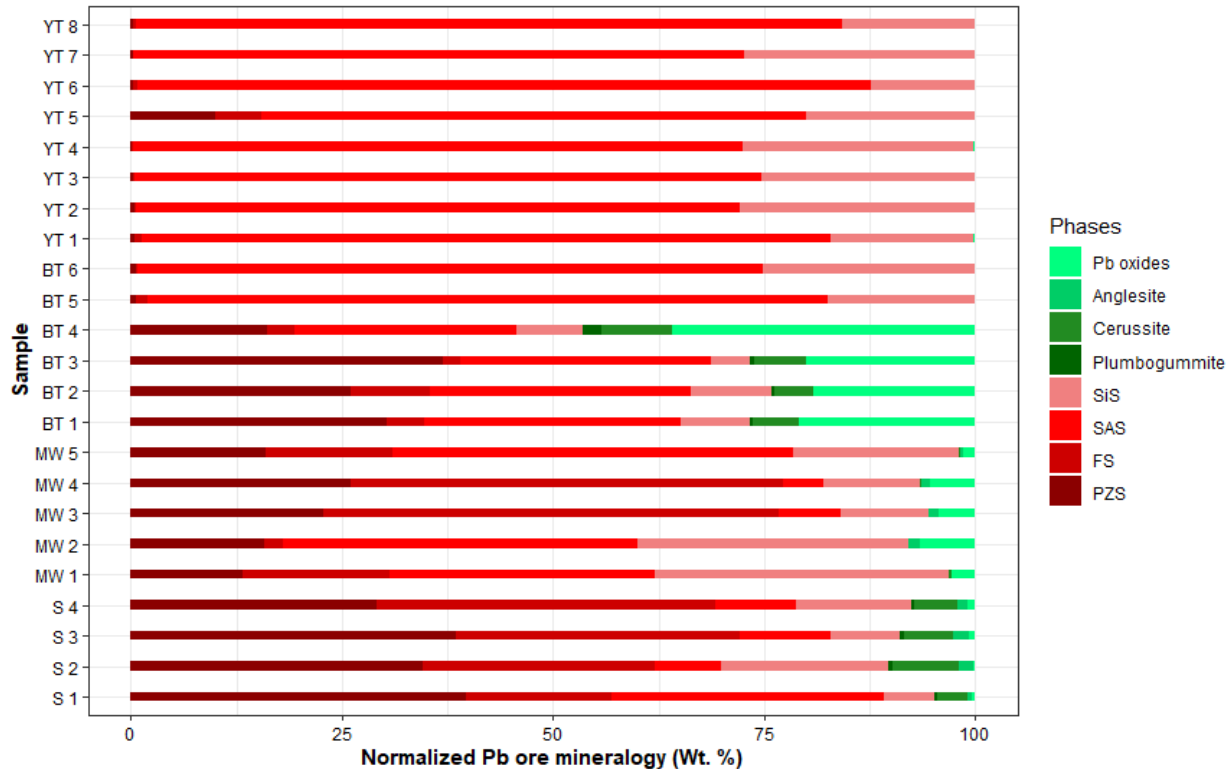
Figure 5. Median abundances of the Pb-bearing minerals and slags, given by bootstrap resampling of the MLA data, normalised to a sum of 100 %. SiS- SiO_2-rich slags; SAS- SiO_2-Al_2O_3-rich slags; FS- Fe_2O_3-rich slags; PZS- PbO-ZnO-rich slags.

All the Pb-bearing phases with contents higher than 1 wt. % showed RSD lower than 15 %, often even lower than 10 %. However, all the phases with contents lower than 1 wt. % showed high RSD (53-95 %). In general, the lower the content of the Pb-bearing phase, the higher the uncertainty regarding its abundance (A4 in ESM 1).

Median lead deportments (Figure 6) indicate that lead is hosted in rather variable proportions by different types of slags, Pb oxides, anglesite, cerussite and plumbogummite. Slags are the most relevant Pb-bearing phase for soils (45-60 %) and yellow tailings (88-100 %). For soil, lead is hosted dominantly by PZS, while SAS are the most important source of lead for yellow tailings. In soils, the remaining lead is predominantly hosted by anglesite (23-37 %), cerussite (5-13 %) and Pb oxides (1- 6 %). Pb oxide (70-80 %) is the most important host of lead for brown tailings (Figure 6). The remaining lead is hosted by anglesite (15-17 %) and different types of slags (3-15 %). In two samples of brown tailings, PZS and Pb oxides contribute equally to the total lead content. As mentioned above, in yellow tailings, slags are the major or only host of lead, with the remaining lead hosted by Pb oxide (0-11 %) (Figure 6). The median calculated lead deportment for metallurgical waste samples (Figure 6) indicates that lead is distributed rather variably, hosted by PZS (23-47 %) and Pb oxides (40-60 %). The rest of the lead is hosted by cerussite (~8 %), anglesite (~0.7 %), SiS (~0.3 %), SAS (0.5-11 %) and FS (0-16 %) slags (Figure 6).
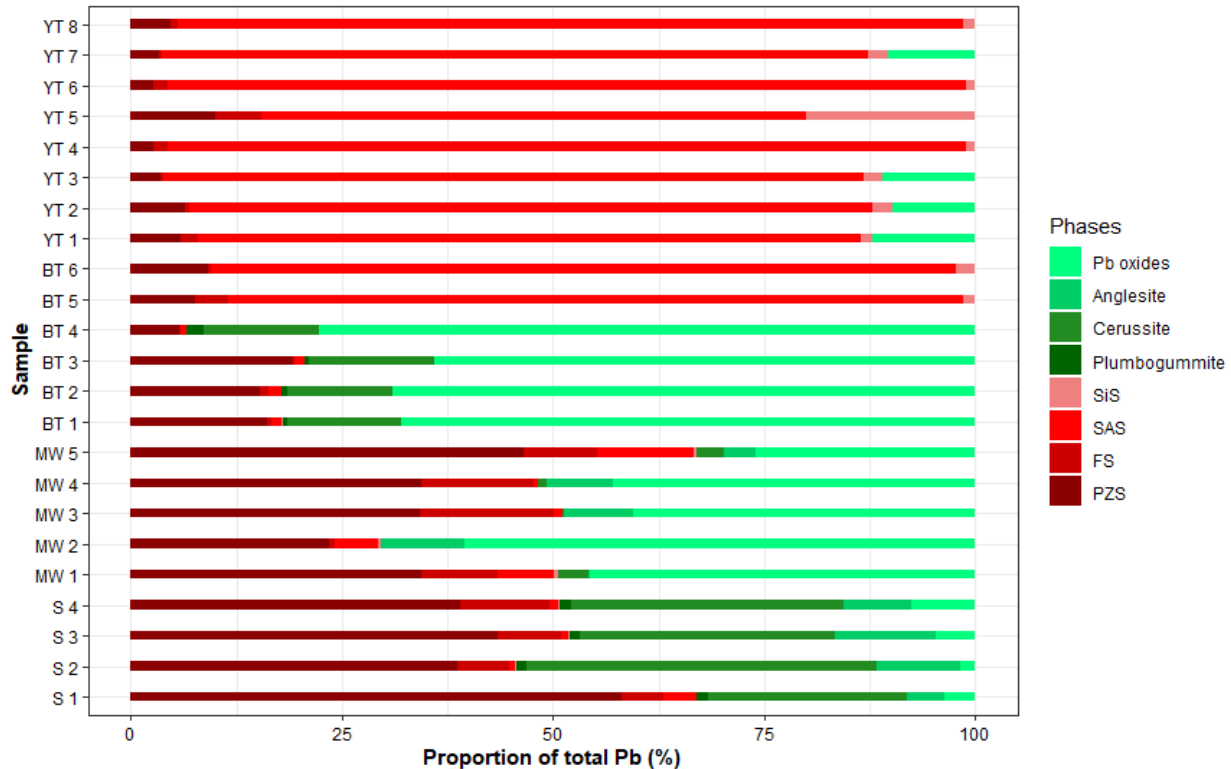
Figure 6. Median lead deportments in the different mine waste samples. SiS- SiO_2-rich slags; SAS- SiO_2-Al_2O_3-rich slags; FS- Fe_2O_3-rich slags; PZS- PbO-ZnO-rich slags.

As could be anticipated, the RSD for lead deportment are closely related to the RSD of the modal and ore mineralogy (Figures A2, A4 in ESM 1). Low RSD (< 10 %) correspond to Pb-bearing phases which are present in higher abundances. The highest RSD in deportment estimations are observed for Pb-bearing minerals in the yellow tailings samples, two samples of brown tailings (BT 5 and BT 6) and for any Pb-bearing phases with a content lower than 1 wt. % regardless of the material (A5 in ESM 1).

3.4. Zinc deportment

The following Zn-bearing minerals were detected with MLA and EPMA: sphalerite (ZnS), smithsonite ($ZnCO_3$), gahnite ($ZnAl_2O_4$), willemite (Zn_2SiO_4), bannisterite ((Ca, K)(Mn^{2+}, Zn, Fe^{2+})$_{10}$(Si, Al)$_{16}O_{38}(OH)_8 \cdot nH_2O$), and fraipontite ((Zn, Al)$_3$(Si, Al)$_2O_5(OH)_4$) (Figure 7). In total, 25 point analyses were collected on these minerals (sphalerite (n = 7), gahnite (n = 9) and willemite (n=9)). EPMA analyses of Zn-bearing phases can be found in Table A8. Point analyses on calcite revealed Zn contents of up to 400 ppm. However, in most cases, zinc concentrations were below the detection limit (d.l. <210 ppm). In some pyrite grains, the zinc content is elevated along the rims of the grains (Figure A6). In most of the pyrite grains, however, zinc was not detected. The contributions of calcite and pyrite to zinc deportment are negligible in all samples, and they were left out of the deportment calculations.

In the soil and metallurgical waste samples, the most abundant zinc phases are fraipontite (1-23 wt. %), SiS (2-14 wt. %), SAS (1-32 wt. %), FS (1-32 wt. %) and PZS (5-16 wt. %) (Figure 9 and Table A6.). Other minerals present within these two materials are willemite (0.1 to 2.9 wt. %) and gahnite (1 to 2.4 wt. %). In both types of tailings, SiS and SAS slags represent more than 90 % of the Zn-bearing phases, the other

380 two types of slags are present in minor contents (< 2 %). Bannisterite and sphalerite are the only Zn-
381 bearing minerals found within the tailings material, which host only ~ 3 % of zinc.

382
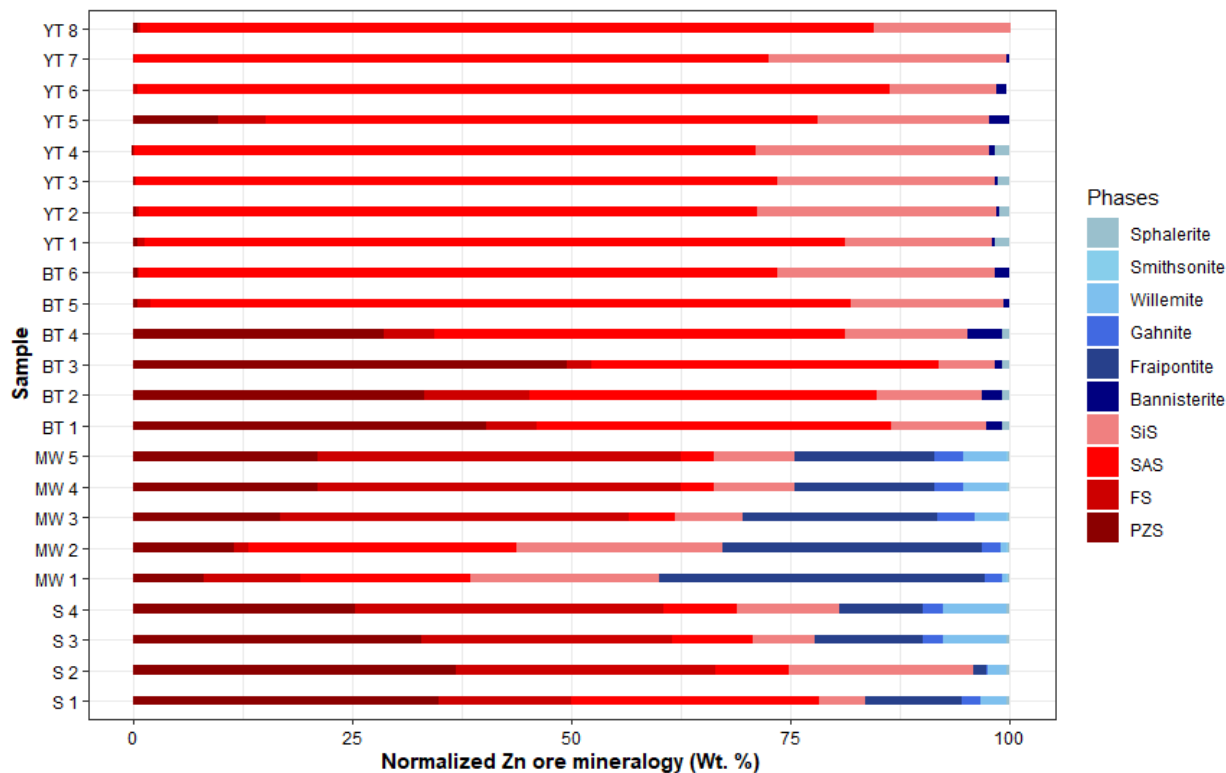
Figure 7. Modal abundances of the Zn-bearing phases, given by bootstrap resampling of the MLA data,
normalised to a sum of 100 %. SiS- SiO_2-rich slags; SAS- SiO_2-Al_2O_3-rich slags; FS- Fe_2O_3-rich slags; PZS- PbO-
ZnO-rich slags.

386 Before the zinc deportment was calculated, the RSDs of the contents of the Zn-bearing phases were
387 established (Figure A7 in ESM 1). The highest RSDs occur for the phases with contents of ≤ 1 wt. %, for
388 both modal mineralogy and zinc deportment (Figure A7 and A8 in ESM 1). The RSD range from 25 % up 82
389 %, depending on the material. The highest RSD are seen for sphalerite and bannisterite in the tailings
390 samples. For the phases with contents higher than 1 wt. %, RSD are lower than 15 % (Figure A7 in ESM 1).

391 Median zinc deportments (Figure 8) indicate that different types of slags are the main hosts of the zinc in
392 soil and the two types of tailings. For soil and brown tailings, the lead-zinc slags (44-91 %) are the major
393 source of zinc. In soils, the rest of the zinc content is distributed between willemite (1-27 %), gahnite (3-5
394 %) and fraipontite (9-37 %). In both types of tailings, the remaining zinc is distributed between bannisterite
395 and sphalerite (0-3 %). In yellow tailings, iron (82-91 %) slags are the major host of zinc. The median
396 calculated zinc department for metallurgical waste samples (Figure 8) indicates that zinc is hosted rather
397 variably by fraipontite (35-76 %) and PZS (20-35 %). The rest of zinc is distributed between willemite (1-
398 15 %), gahnite (3-7 %), SiS (~0.5 %), SAS (0.5-4.3 %) and FS (0.3-2 %) (Figure 8).

399
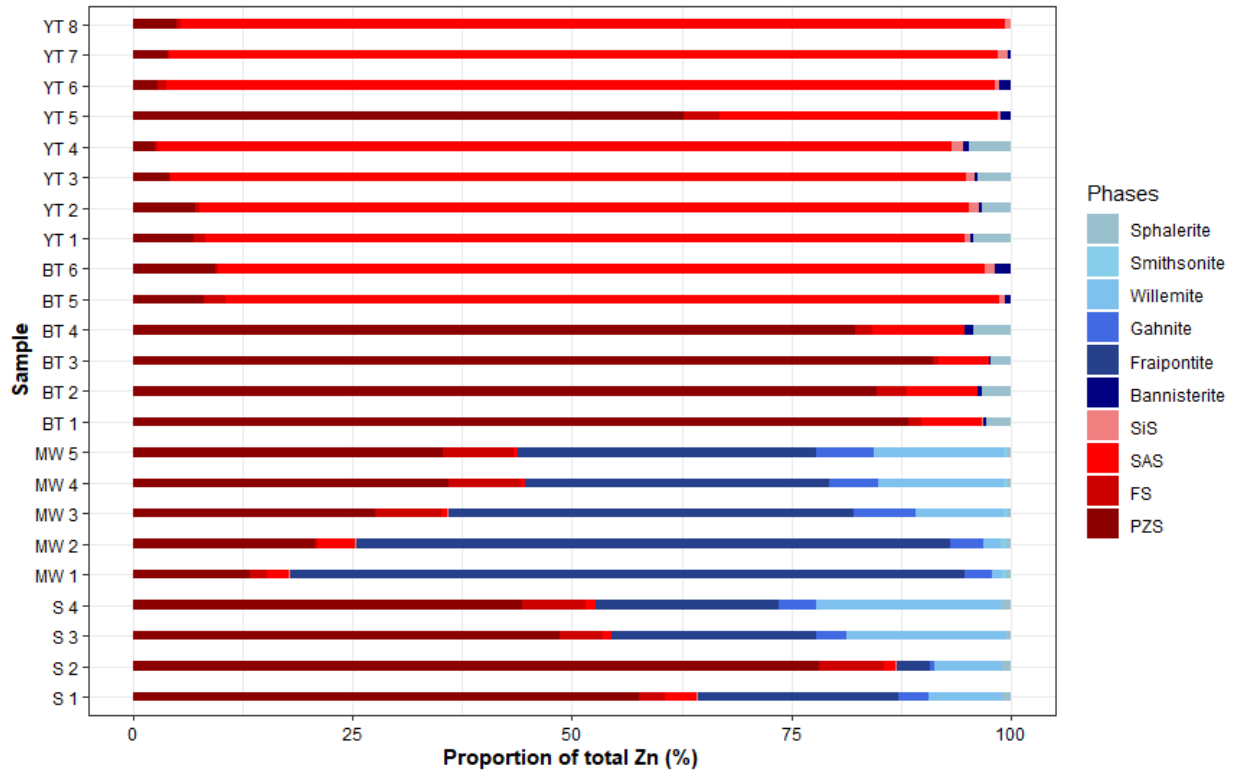
Figure 8. Distribution of zinc across different Zn-bearing phases in the different mine waste samples. SiS-
SiO$_2$-rich slags; SAS- SiO$_2$-Al$_2$O$_3$-rich slags; FS- Fe$_2$O$_3$-rich slags; PZS- PbO-ZnO-rich slags.

Comparable to the lead deportment uncertainties, the highest uncertainties for zinc deportment are
closely related to the high uncertainties of the low content of Zn-bearing phases (Figure A8 ESM 1). The
RSDs are lower than 15 % for all Zn-bearing phases that have a content higher than 1 wt. % (most often
lower than 10 %) (Figure A8 ESM 1). For phases with a content lower than 1 wt. %, RSDs vary from 60 up
to 127 % (Figure A8 ESM 1).

3.5. Data quality

To assess the quality and reliability of MLA measurements combined with EPMA, calculated Pb and Zn
grades for each sample were compared with the chemical assays measured at an external laboratory.
Despite the variable mineralogy and the complex chemistry of the slags, the general agreement between
the measured and calculated assays for lead and zinc are very good (Figure 9). The calculated lead and/or
zinc contents showed systematically high RSD for samples with overall low contents of lead and/or zinc
and for the samples where slags are the major source of the metal.
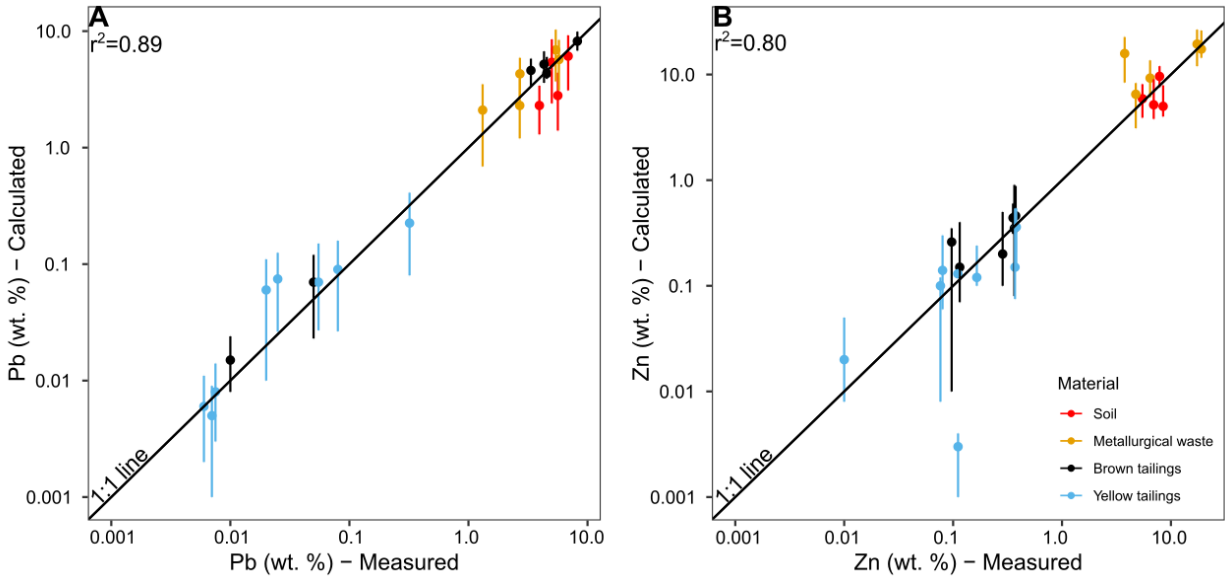
Figure 9. Correspondence between calculated lead (left) and zinc (right) content from MLA and EPMA (vertical axis) and measured bulk lead (left) and zinc (right) concentration measured by XRF (horizontal axis).

Even though the materials under study are complex and heterogeneous, the coefficients of correlation are relatively high, 0.89 and 0.80 for lead and zinc, respectively. For lead, all calculated grades plot on the 1:1 line within the error (Figure 9). In contrast, for zinc, not all samples fall on the 1:1 line (Figure 9), with one sample of yellow tailings being significantly under-estimated and one sample of metallurgical waste being over-estimated. However, there is no systematic deviation of the data from the 1:1 line.

As mentioned above, the highest RSD occur for samples with low lead and zinc content. For example, the median value of the calculated Pb content in sample BT1 is 3.9 wt. %, with the 95% confidence interval ranging from 3.8 to 4.1 wt. %. This corresponds to an RSD of less than 10 %. For BT 5, on the other hand, the median calculated Pb content is 0.07 wt. %, with a 95% confidence interval of 0.02 to 0.12 wt. %. This corresponds to an RSD of approximately 70 %.

In addition to the samples with low lead and zinc contents, samples where slags are the major lead and zinc sources also have high RSDs. For instance, in all soil samples, PZS and cerussite in particular, as well as Pb oxides and other types of slags, have RSD ranging from 45 to 55 %. The highest RSDs of all occur in samples where low lead and zinc contents coincide with slags being the major host of these metals, e.g. yellow tailings, where RSDs range from 67 up to 90 % for lead and from 40 up to 167 % for zinc (Figure 9). The chemical heterogeneity of slags clearly exacerbates the nugget effect when the contents of the slags are low.

4. Discussion

The following section discusses the need for an integrated approach for characterising mine waste materials, particularly metal deportment. Following this, the implications of the findings will be assessed with regard to suitable processing routes.

4.1. The need for an integrated approach

Mineralogical deportments of a metals are well known to be some of the key pieces of information required to improve and maximise metal recoveries from ores (Frenzel et al., 2019). Accurately estimating deportment can be a challenging task, even with simple mineral phases. With the addition of non-mineral phases (e.g., slags), the calculations become even increasingly complex and challenging. This is directly related to the compositional heterogeneity of slags.

Traces of lead-bearing minerals (cerussite and anglesite) were previously identified in soil, metallurgical waste and brown tailing samples by XRD, but were not detected in yellow tailings (Bevandić et al., 2021). Regarding the zinc-bearing minerals, XRD analysis identified franklinite and willemite in metallurgical waste, but not in the tailings or soils (Bevandić et al., 2021). However, in these samples franklinite was not observed when using the MLA/EPMA approach. Instead, gahnite ($ZnAl_2O_4$) was identified, and this occurred due to the similarity in XRD patterns making them hard to distinguish. The crystal structure and lattice parameters of these minerals are similar, however gahnite has a significantly higher zinc content. Therefore, it was important to establish whether gahnite and/or franklinite were present, and in which abundance(s), to more accurately estimate mineral deportment (Levy et al., 2001; Reichmann et al., 2008). This clearly shows the benefit of using MLA combined with EPMA. The integrated approach used in this study detected other lead- and zinc-bearing phases that were not identified by XRD. With MLA, more lead- and zinc-bearing phases were detected than with XRD, including those present in trace contents and in material types where no Pb- and Zn-phases were previously identified (e.g. Pb oxides in yellow tailings and sphalerite in brown tailings). Even abundant zinc minerals, such as fraipontite in metallurgical waste, were not detected with the XRD. This is connected to the limitation of analysis with XRD. For example, both willemite and Zn spinels (e.g. gahnite, franklinite) are easy to detect with XRD, contrary to some other phases such as fraipontite and bannisterite (Manceau et al., 2000; Roberts et al., 2002; Baker et al., 2012).

Although MLA provides valuable and quantitative data that could not have been obtained with only XRD, the measurements are more time consuming, costly and require significant user input and decision making which may lead to bias in the results. For instance, the extraction of relevant X-ray spectra to build the mineral/phase list used to classify the minerals present is not required for XRD when analysing common minerals. A similar procedure would in fact be required if the aim of the XRD was to quantify slag phases, but this would be greatly complicated by the complex and inter-grown nature of the slag phases (Zhao et al., 2018). Therefore, this study has clearly demonstrated that the extra time and cost is justifiable when considering that the main Zn- and Pb-bearing phases could not be accurately identified or quantified with XRD.

Both of these factors are highly important for assessing metal deportment, particularly the distribution of lead and zinc between mineral and slag phases in this case. This information has highlighted the differences between the four mine waste material types at the Plombières tailing pond and has an important bearing on the potential for processing and metal recovery, or environmental implications, of the materials.

Importantly, the approach used here is applicable for different types of mine waste, including tailings, topsoil, waste rock and slags. This has been confirmed during this study, by applying the same procedure to four types of mine waste with different mineralogical and geochemical characteristics. However, the

481 discrepancy in the calculated and measured lead and zinc contents for samples with low abundances of
482 these metals is noticeable. This is related to a low number of Pb- and Zn-bearing mineral grains, which
483 results in a nugget effect and thus high variability occurs in the calculated assay (Blannin et al., 2021)
484 (Figure 9).

485 4.2. Potential for re-processing of the material
486 Numerous studies have proved how the application of automated mineralogical methods was beneficial
487 for tailoring suitable processing routes for primary, but also secondary sources of metals such as mine and
488 technological waste like lithium-ion batteries (e.g. Santoro et al., 2014; Holley et al., 2018; Barton et al.,
489 2018; Xu et al., 2019; Schulz et al., 2020; Mulenshi et al., 2021; Vanderbruggen et al., 2021). The benefits
490 of applying automated mineralogy methods on mine and urban wastes are related to the possibility to
491 characterize complex materials that consist of mineral and non-mineral phases, which are problematic for
492 characterization with standard mineralogical methods (Lapakko, 2002; Matinde et al., 2018; Schulz et al.,
493 2020; Vanderbruggen et al., 2021;).

494 Selecting an optimum route for the extraction of both lead and zinc from the Plombières mine waste is a
495 challenging task due to the complex mineralogical nature of the materials, a feature common for many
496 mine wastes (Lapakko, 2002; Matinde et al., 2018). Furthermore, reprocessing of the mine waste for
497 secondary metal recovery should focus on multiple elements rather than a single element (Escobar et al.,
498 2021; Taha et al., 2021). Recent studies on different mine waste materials have established that
499 hydrometallurgical approaches are more suitable than pyrometallurgical processes for the extraction of
500 lead and zinc (Xanthopoulos et al., 2017; Mohanty et al., 2018; Makua et al., 2019; Rodriguez et al., 2020).
501 Since the Plombières material consists of both mineral and non-mineral phases, which are equally
502 important sources of lead and zinc, only hydrometallurgical methods are applicable and will be further
503 discussed.

504 As suggested by Bevandić et al. (2021b), extraction of metals should be from the metallurgical waste layer
505 and brown tailings, which have the highest lead and zinc contents. Having several sources of lead and zinc,
506 the material studied may require different extraction methods to maximise metal recovery. The presence
507 of the Zn-bearing clay mineral fraiponite as the major source of zinc in the metallurgical waste layer will
508 require a step of de-sliming prior to leaching, to maximise recovery of zinc and optimise liberation
509 (Choulet et al., 2016). Leaching with sulphuric acid was shown to be highly suitable for samples that consist
510 of different types of Zn-bearing phases (e.g. sulphides, oxides, silicates) found within the Plombières mine
511 waste material (Moradi and Monhemius, 2011). However, sulphuric acid is unsuitable for the extraction
512 of lead, which would be precipitated as anglesite (Zhang et al., 2019; Bevandic et al., 2021b) and extraction
513 of lead and zinc from slags is not efficient due to its amorphous structure of it (Banza et al., 2002; Bevandic
514 et al., 2021b). This would increase the price of lead extraction by requiring an additional step to recover
515 lead from the leaching residues. Additionally, iron is highly leachable with acid-based lixiviants with a pH
516 lower than 4. Iron is an undesirable metal in the pregnant leaching solution (PLS), and would therefore
517 necessitate iron removal from the solution (Bevandic et al., 2021b), thus increasing costs. Another lixiviant
518 that can be excluded for extraction of metals from Plombières mine waste is ammonia/ammonium
519 carbonate, which showed to be unsuitable for the extraction of zinc from silicates such as willemite
520 (Aletan, 1968; Moradi and Monhemius, 2011).

521 Alternatively, alkaline lixiviants (e.g. sodium hydroxide) were shown to be more suitable than acid-based
522 (e.g. sulphuric acid) for metal extraction of both lead and zinc from mine waste samples (Bevandic et al.,

523 2021), especially if the samples are roasted beforehand (Atia and Spooren, 2020). Sodium hydroxide was
524 demonstrated to be one of the most efficient lixiviants for the extraction of lead and zinc from mine waste
525 material (Ghasemi and Azizi, 2018). It would be suitable for the extraction of both lead and zinc from most
526 minerals found in the Plombières mine waste materials, as well as the slag phases (Shibayama et al., 2010;
527 Ghasemi and Azizi, 2018). Additionally, the use of sodium hydroxide as a lixiviant does not result in the
528 leaching of iron, and therefore no additional iron removal step would be required. However, at present,
529 there is no information about the efficiency of sodium hydroxide for the extraction of zinc from clay
530 minerals (e.g. fraiponite). Both, sulfuric acid and sodium hydroxide are relatively cheap lixiviants when
531 compared to other lixiviants (e.g. methanesulfonic acid) used for extraction of lead and zinc.

532 Bevandić et al. (2021b) showed that H_2SO_4 and methanesufonic acid (MSA) are not suitable lixiviants for
533 extraction of metals from Plombières mine waste, due to high leaching of iron and formation of new lead-
534 and zinc-bearing phases. Sulfuric acid showed to be unsuitable for the extraction of lead, which re-
535 precipitated as anglesite (Zhang et al., 2019; Bevandić et al., 2021b), while MSA showed to be unsuitable
536 for the extraction of Zn, which re-precipitated as simonkolleite ($Zn_5(OH)_8Cl_2 \cdot H_2O$). Sodium hydroxide was
537 demonstrated to be one of the most efficient lixiviants for the extraction of lead and zinc from Plombières
538 mine waste material (Ghasemi and Azizi, 2018; Atia and Spooren, 2020). Additionally, the use of sodium
539 hydroxide as a lixiviant does not result in the leaching of iron, and therefore no additional iron removal
540 step would be required (Bevandić et al., 2021b). The same study concluded that extraction of lead and
541 zinc from slags is not efficient without pre-treatment of the samples (Bevandić et al., 2021b).

542 It is worth mentioning that textural information (e.g. liberation of grains, grain size) are an important
543 controlling factor for re-processing of the material. Textural data can be obtained from MLA but the
544 integration of MLA and EPMA data to accurately characterise the metal deportment was deemed more
545 important at this stage and was, therefore the focus of this study. With the complete overview of the
546 mineralogy and deportment in this study, a systematic approach can be applied to assess the applicability
547 of specific methods and to work towards a flow sheet that maximises the recovery of metals. Future work
548 should focus on using automated mineralogical methods to optimise conditions for extraction of the
549 metals of interest from both mineral and slag phases. This would be achieved by applying methods such
550 as MLA on the residue after the leaching tests are performed and observe how the mineralogical and
551 textural properties are influenced by leaching.

552 ## 5. Conclusion
553 The work conducted in this study, which is the first of its kind applied to Plombières mine wastes, provides
554 a detailed quantitative chemical characterisation of different mine waste materials found within the
555 Plombières tailing pond. The integrated approach used in this study demonstrated that significant
556 amounts of lead and zinc are hosted in slag phases (23-100 %). The rest is hosted in minerals (0-76 %) that
557 are present in low abundances such as Pb oxides, anglesite, cerussite for lead and fraipontite, willemite
558 and gahnite for zinc. It is important that these minerals and phases are identified and quantified to provide
559 an accurate understanding of the metal deportment which can be used to assess the potential
560 reprocessing routes for the recovery of lead and zinc from the mine wastes.

561 Despite the heterogeneity of the mine wastes at the studied site, deportment estimations had acceptable
562 uncertainties for the soil, metallurgical waste and most of the brown tailings samples. However, samples
563 with low lead and zinc contents showed higher uncertainties, assumed to be in relation to the nugget
564 effect. As demonstrated, acceptable results can be obtained from low-grade, but also heterogeneous

565 mine waste material. These promising findings are expected for other mine waste deposits around the
566 globe.

567 As we turn towards re-mining and the recovery of metals from mine wastes, metal deportment studies
568 should become the norm to determine the most appropriate processing techniques to be applied and
569 whether there is sufficient economic potential for re-mining.

570 <div align="center">Declarations</div>

576 **Conflicts of interest**: The authors have no conflicts of interest to declare that are relevant to the content
577 of this article.

578 **Authors' contribution**:

579 **Srećko Bevandić**: Conceptualization, Sampling, Methodology, Validation Investigation, Data curation,
580 processing and analysis, Writing - original draft, Writing - review & editing, Visualization. **Rosie Blannin**:
581 Methodology, Validation, Writing - review & editing, Visualization. **Alexandra Gomez Escobar**: Writing -
582 review & editing. **Kai Bachmann**: Measurements, Writing - review & editing, Supervision. **Max Frenzel**:
583 Visualization, Conceptualization, Validation, Writing - review & editing, Supervision. **Álvaro Pinto:** Writing
584 - review & editing, Supervision. **Jorge M. R. S. Relvas:** Writing - review & editing, Supervision. **Philippe
585 Muchez:** Conceptualization, Sampling, Validation, Writing - review & editing, Supervision

586 **Acknowledgements**

590 ## Literature

591 Abo Atia, T., Spooren, J., 2020. Microwave assisted chloride leaching of zinc plant residues. J. Hazard.
592   Mater. 398, 122814. https://doi.org/10.1016/j.jhazmat.2020.122814

593 Amar, H., Benzaazoua, M., Edahbi, M., Villeneuve, M., Joly, M.A., Elghali, A., 2021. Reprocessing
594   feasibility of polymetallic waste rock for cleaner and sustainable mining. J. Geochemical Explor.
595   220, 106683. https://doi.org/10.1016/j.gexplo.2020.106683

596 Aletan, G., 1968. Ammonia leaching of oxidized lead-zinc ores of Iran. Geological Survey of Iran Reports,
597   vol. 15. pp. 19–66

598 Bachmann, K., Frenzel, M., Krause, J., Gutzmer, J., 2017. Advanced Identification and Quantification of
599   In-Bearing Minerals by Scanning Electron Microscope-Based Image Analysis. Microsc. Microanal.
600   23, 527–537. https://doi.org/10.1017/S1431927617000460

601 Baele, J.-M., Bouzahzah, H., Papier, S., Decrée, S., Verheyden, S., Burlet, C., Pirard, E., Franceschi, G.,

602 Dejonghe, L., 2021. Trace-element imaging at macroscopic scale in a Belgian sphalerite-galena ore
603 using Laser-Induced Breakdown Spectroscopy (LIBS). Geol. Belgica 24, 125–136.
604 https://doi.org/10.20341/gb.2021.003

605 Baker, L.R., Pierzynski, G.M., Hettiarachchi, G.M., Scheckel, K.G., Newville, M., 2012. Zinc Speciation in
606 Proximity to Phosphate Application Points in a Lead/Zinc Smelter–Contaminated Soil. J. Environ.
607 Qual. 41, 1865–1873. https://doi.org/10.2134/jeq2012.0168

608 Banza, A.N., Gock, E., Kongolo, K., 2002. Base metals recovery from copper smelter slag by oxidising
609 leaching and solvent extraction. Hydrometallurgy 67, 63–69. https://doi.org/10.1016/S0304-
610 386X(02)00138-X

611 Barton, I., Ahn, J., Lee, J., 2018. Mineralogical and metallurgical study of supergene ores of the Mike Cu–
612 Au(–Zn) deposit, Carlin trend, Nevada. Hydrometallurgy 176, 176–191.
613 https://doi.org/10.1016/j.hydromet.2018.01.022

614 Bevandić, S., Blannin, R., Auwera, J. Vander, Delmelle, N., Caterina, D., Nguyen, F., Muchez, P., 2021a.
615 Geochemical and mineralogical characterisation of historic zn–pb mine waste, plombières, East
616 Belgium. Minerals 11, 1–27. https://doi.org/10.3390/min11010028

617 Bevandić, S., Xanthopoulos, P., Muchez, P., 2021b. Chemical Leaching of Sulfidic Mining Waste,
618 Plombières Tailings Pond, Eastern Belgium: Insights from a Mineralogical Approach. J. Sustain.
619 Metall. 7, 1444–1455. https://doi.org/10.1007/s40831-021-00445-0

620 Blannin, R., Frenzel, M., Tuşa, L., Birtel, S., Ivăşcanu, P., Baker, T., Gutzmer, J., 2021. Uncertainties in
621 quantitative mineralogical studies using scanning electron microscope-based image analysis.
622 Miner. Eng. 167. https://doi.org/10.1016/j.mineng.2021.106836

623 Cabała, J., Warchulski, R., Rozmus, D., Środek, D., Szełęg, E., 2020. Pb-rich slags, minerals, and pollution
624 resulted from a medieval ag-pb smelting and mining operation in the silesian-cracovian region
625 (Southern Poland). Minerals 10. https://doi.org/10.3390/min10010028

626 Ceniceros-Gómez, A.E., Macías-Macías, K.Y., de la Cruz-Moreno, J.E., Gutiérrez-Ruiz, M.E., Martínez-
627 Jardines, L.G., 2018. Characterization of mining tailings in México for the possible recovery of
628 strategic elements. J. South Am. Earth Sci. 88, 72–79.
629 https://doi.org/10.1016/j.jsames.2018.08.013

630 Choulet, F., Buatier, M., Barbanson, L., Guégan, R., Ennaciri, A., 2016. Zinc-rich clays in supergene non-
631 sulfide zinc deposits. Miner. Depos. 51, 467–490. https://doi.org/10.1007/s00126-015-0618-8

632 Dejonghe, Léon ; Ladeuze, France ; Jans, D., 1993. 1993-AtlasGisementsPbZnSynclinVerviers-
633 MemoireSGB33.

634 Dold, B., 2020. Sourcing of critical elements and industrial minerals from mine waste – The final
635 evolutionary step back to sustainability of humankind? J. Geochemical Explor. 219, 106638.
636 https://doi.org/10.1016/j.gexplo.2020.106638

637 EA (Environment Agency), 2009. Human health toxicological assessment of contaminants in soil,
638 Environment Agency.

639 Elghali, A., Benzaazoua, M., Bouzahzah, H., Abdelmoula, M., Dynes, J.J., Jamieson, H.E., 2021. Role of
640 secondary minerals in the acid generating potential of weathered mine tailings: Crystal-chemistry
641 characterization and closed mine site management involvement. Sci. Total Environ. 784, 147105.

642 https://doi.org/10.1016/j.scitotenv.2021.147105

643

644 Elghali, A., Benzaazoua, M., Bouzahzah, H., Bussière, B., Villarraga-Gómez, H., 2018. Determination of
645 the available acid-generating potential of waste rock, part I: Mineralogical approach. Appl.
646 Geochemistry 99, 31–41. https://doi.org/10.1016/j.apgeochem.2018.10.021

647 Escobar, A.G., Relvas, J.M.R.S., Pinto, Á.M.M., Oliveira, M., 2021. Physical–Chemical Characterization of
648 the Neves Corvo Extractive Mine Residues: A Perspective Towards Future Mining and Reprocessing
649 of Sulfidic Tailings. J. Sustain. Metall. 7, 1483–1505. https://doi.org/10.1007/s40831-021-00428-1

650 Ettler, V., 2015. Soil contamination near non-ferrous metal smelters: A review. Appl. Geochemistry 64,
651 56–74. https://doi.org/10.1016/j.apgeochem.2015.09.020

652 Evans, C.L., Napier-Munn, T.J., 2013. Estimating error in measurements of mineral grain size distribution.
653 Miner. Eng. 52, 198–203. https://doi.org/10.1016/j.mineng.2013.09.005

654 Falagán, C., Grail, B.M., Johnson, D.B., 2017. New approaches for extracting and recovering metals from
655 mine tailings. Miner. Eng. 106, 71–78. https://doi.org/10.1016/j.mineng.2016.10.008

656 Fandrich, R., Gu, Y., Burrows, D., Moeller, K., 2007. Modern SEM-based mineral liberation analysis. Int. J.
657 Miner. Process. 84, 310–320. https://doi.org/10.1016/j.minpro.2006.07.018

658 Frenzel, M., Bachmann, K., Carvalho, J.R.S., Relvas, J.M.R.S., Pacheco, N., Gutzmer, J., 2019. The
659 geometallurgical assessment of by-products—geochemical proxies for the complex mineralogical
660 deportment of indium at Neves-Corvo, Portugal. Miner. Depos. 54, 959–982.
661 https://doi.org/10.1007/s00126-018-0849-6

662 Gómez-Arias, A., Yesares, L., Caraballo, M.A., Maleke, M., Vermeulen, D., Nieto, J.M., van Heerden, E.,
663 Castillo, J., 2021. Environmental and geochemical characterization of alkaline mine wastes from
664 Phalaborwa (Palabora) Complex, South Africa. J. Geochemical Explor. 224.
665 https://doi.org/10.1016/j.gexplo.2021.106757

666 Gregory, M.J., Lang, J.R., Gilbert, S., Hoal, K.O., 2013. Geometallurgy of the Pebble porphyry copper-
667 gold-molybdenum deposit, Alaska: Implications for gold distribution and paragenesis. Econ. Geol.
668 108, 463–482. https://doi.org/10.2113/econgeo.108.3.463

669 Guanira, K., Valente, T.M., Ríos, C.A., Castellanos, O.M., Salazar, L., Lattanzi, D., Jaime, P., 2020.
670 Methodological approach for mineralogical characterization of tailings from a Cu(Au,Ag) skarn type
671 deposit using QEMSCAN (Quantitative Evaluation of Minerals by Scanning Electron Microscopy). J.
672 Geochemical Explor. 209, 106439. https://doi.org/10.1016/j.gexplo.2019.106439

673 Heinig, T., Bachmann, K., Tolosana-Delgado, R., Van Den Boogaart, G., Gutzmer, J., 2015. Monitoring
674 gravitational and particle shape settling effects on MLA sampling preparation. Proc. IAMG 2015 -
675 17th Annu. Conf. Int. Assoc. Math. Geosci. 200–206.

676 Helser, J., Cappuyns, V., 2021. Trace elements leaching from Pb[sbnd]Zn mine waste (Plombières,
677 Belgium) and environmental implications. J. Geochemical Explor. 220, 106659.
678 https://doi.org/10.1016/j.gexplo.2020.106659

679 Hesse, M., Popov, O., Lieberwirth, H., 2017. Increasing efficiency by selective comminution. Miner. Eng.
680 103–104, 112–126. https://doi.org/10.1016/j.mineng.2016.09.003

681 Holley, E.A., Yu, Y.T., Navarre-Sitchler, A., Winterton, J., 2018. Quantitative mineralogy and geochemistry
682   of pelletized sulfide-bearing gold concentrates in an alkaline heap leach. Hydrometallurgy 181,
683   130–142. https://doi.org/10.1016/j.hydromet.2018.06.017

684 Horckmans, L., Möckel, R., Nielsen, P., Kukurugya, F., Vanhoof, C., Morillon, A., Algermissen, D., 2019.
685   Multi-analytical characterization of slags to determine the chromium concentration for a possible
686   re-extraction. Minerals 9, 1–14. https://doi.org/10.3390/min9100646

687 Hudson-Edwards, K.A., Jamieson, H.E., Lottermoser, B.G., 2011. Mine wastes: Past, present, future.
688   Elements 7, 375–380. https://doi.org/10.2113/gselements.7.6.375

689 Jamieson, H.E., Walker, S.R., Parsons, M.B., 2015. Mineralogical characterization of mine waste. Appl.
690   Geochemistry 57, 85–105. https://doi.org/10.1016/j.apgeochem.2014.12.014

691 Karaca, O., Cameselle, C., Reddy, K.R., 2017. Acid pond sediment and mine tailings contaminated with
692   metals: physicochemical characterization and electrokinetic remediation. Environ. Earth Sci. 76, 1–
693   12. https://doi.org/10.1007/s12665-017-6736-0

694 Kern, M., Möckel, R., Krause, J., Teichmann, J., Gutzmer, J., 2018. Calculating the deportment of a fine-
695   grained and compositionally complex Sn skarn with a modified approach for automated
696   mineralogy. Miner. Eng. 116, 213–225. https://doi.org/10.1016/j.mineng.2017.06.006

697 Kucha, H., Martens, A., Ottenburgs, R., De Vos, W., Viaene, W., 1996. Primary minerals of Zn-Pb mining
698   and metallurgical dumps and their environmental behavior at Plombieres, Belgium. Environ. Geol.
699   27, 1–15. https://doi.org/10.1007/BF00770598

700 Kuhn, K., Meima, J.A., 2019. Characterization and economic potential of historic tailings from gravity
701   separation: Implications from a mine waste dump (PB-AG) in the Harz mountains mining district,
702   Germany. Minerals 9. https://doi.org/10.3390/min9050303

703 Lapakko, K., 2002. Metal mine rock and waste characterization tools: An overview. Int. Inst. Environ.
704   Dev. 2002.

705 Levy, D., Pavese, A., Sani, A., Pischedda, V., 2001. Structure and compressibility of synthetic ZnAl2O4
706   (gahnite) under high-pressure conditions, from synchrotron X-ray powder diffraction. Phys. Chem.
707   Miner. 28, 612–618. https://doi.org/10.1007/s002690100194

708 Lindsay, M.B.J., Moncur, M.C., Bain, J.G., Jambor, J.L., Ptacek, C.J., Blowes, D.W., 2015. Geochemical and
709   mineralogical aspects of sulfide mine tailings. Appl. Geochemistry 57, 157–177.
710   https://doi.org/10.1016/j.apgeochem.2015.01.009

711 Liu, Z., Shao, Y., Zhou, H., Liu, N., Huang, K., Liu, Q., Zhang, J., Wang, C., 2018. Major and trace element
712   geochemistry of pyrite and pyrrhotite from stratiform and lamellar orebodies: Implications for the
713   ore genesis of the dongguashan copper (gold) deposit, Eastern China. Minerals 8.
714   https://doi.org/10.3390/min8090380

715 Makua, L., Langa, K., Saguru, C., Ndlovu, S., 2019. PGM recovery from a pregnant leach solution using
716   solvent extraction and cloud point extraction: A preliminary comparison. J. South. African Inst. Min.
717   Metall. 119, 453–458. https://doi.org/10.17159/2411-9717/17/484/2019

718 Manceau, A., Marcus, M.A., Tamura, N., 2002. Quantitative speciation of heavy metals in soils and
719   sediments by synchrotron X-ray techniques. Rev. Mineral. Geochemistry 49.
720   https://doi.org/10.2138/gsrmg.49.1.341

721   Mariano, R.A., Evans, C.L., 2015. Error analysis in ore particle composition distribution measurements.
722   Miner. Eng. 82, 36–44. https://doi.org/10.1016/j.mineng.2015.06.001

723   Martínez, J., Hidalgo, M.C., Rey, J., Garrido, J., Kohfahl, C., Benavente, J., Rojas, D., 2016. A
724   multidisciplinary characterization of a tailings pond in the Linares-La Carolina mining district, Spain.
725   J. Geochemical Explor. 162, 62–71. https://doi.org/10.1016/j.gexplo.2015.12.013

726   Matinde, E., Simate, G.S., Ndlovu, S., 2018. Mining and metallurgical wastes: A review of recycling and
727   re-use practices. J. South. African Inst. Min. Metall. 118, 825–844. https://doi.org/10.17159/2411-
728   9717/2018/v118n8a5

729   Mikulski, S.Z., Oszczepalski, S., Sadłowska, K., Chmielewski, A., Małek, R., 2020. Trace element
730   distributions in the Zn-Pb (Mississippi valley-type) and Cu-Ag (Kupferschiefer) sediment-hosted
731   deposits in Poland. Minerals 10. https://doi.org/10.3390/min10010075

732   Minz, F.E., Bolin, N.J., Lamberg, P., Bachmann, K., Gutzmer, J., Wanhainen, C., 2015. Distribution of Sb
733   minerals in the Cu and Zn flotation of Rockliden massive sulphide ore in north-central Sweden.
734   Miner. Eng. 82, 125–135. https://doi.org/10.1016/j.mineng.2015.03.007

735   Mohanty, U.S., Rintala, L., Halli, P., Taskinen, P., Lundström, M., 2018. Hydrometallurgical approach for
736   leaching of metals from copper rich side stream originating from base metal production. Metals
737   (Basel). 8. https://doi.org/10.3390/met8010040

738   Mondillo, N., Herrington, R., Boyce, A.J., Wilkinson, C., Santoro, L., Rumsey, M., 2018. Critical elements
739   in non-sulfide Zn deposits: a reanalysis of the Kabwe Zn-Pb ores (central Zambia). Mineral. Mag.
740   82, S89–S114. https://doi.org/10.1180/minmag.2017.081.038

741   Moradi, S., Monhemius, A.J., 2011. Mixed sulphide-oxide lead and zinc ores: Problems and solutions.
742   Miner. Eng. 24, 1062–1076. https://doi.org/10.1016/j.mineng.2011.05.014

743   Morrison, A.L., Swierczek, Z., Gulson, B.L., 2016. Visualisation and quantification of heavy metal
744   accessibility in smelter slags: The influence of morphology on availability. Environ. Pollut. 210, 271–
745   281. https://doi.org/10.1016/j.envpol.2015.11.030

746   Mulenshi, J., Gilbricht, S., Chelgani, S.C., Rosenkranz, J., 2021. Systematic characterization of historical
747   tailings for possible remediation and recovery of critical metals and minerals – The Yxsjöberg case.
748   J. Geochemical Explor. 226, 106777. https://doi.org/10.1016/j.gexplo.2021.106777

749   Parbhakar-Fox, A., Fox, N., Jackson, L., Cornelius, R., 2018. Forecasting geoenvironmental risks:
750   Integrated applications of mineralogical and chemical data. Minerals 8, 1–21.
751   https://doi.org/10.3390/min8120541

752   Parbhakar-Fox, A.K., Edraki, M., Walters, S., Bradshaw, D., 2011. Development of a textural index for the
753   prediction of acid rock drainage. Miner. Eng. 24, 1277–1287.
754   https://doi.org/10.1016/j.mineng.2011.04.019

755   Pereira, L., Frenzel, M., Hoang, D.H., Tolosana-Delgado, R., Rudolph, M., Gutzmer, J., 2021a. Computing
756   single-particle flotation kinetics using automated mineralogy data and machine learning. Miner.
757   Eng. 170, 107054. https://doi.org/10.1016/j.mineng.2021.107054

758   Pereira, L., Frenzel, M., Khodadadzadeh, M., Tolosana-Delgado, R., Gutzmer, J., 2021b. A self-adaptive
759   particle-tracking method for minerals processing. J. Clean. Prod. 279, 123711.
760   https://doi.org/10.1016/j.jclepro.2020.123711

761   Poloko, N., Moatlhodi, L.K., Danha, G., 2019. Investigation of mineral deportment in a copper ore from
762   Botswana. IOP Conf. Ser. Mater. Sci. Eng. 641. https://doi.org/10.1088/1757-899X/641/1/012024

763   Rahfeld, A., Gutzmer, J., 2017. MLA-Based Detection of Organic Matter with Iodized Epoxy Resin—An
764   Alternative to Carnauba. J. Miner. Mater. Charact. Eng. 05, 198–208.
765   https://doi.org/10.4236/jmmce.2017.54017

766   Rao, D.S., Das, B., 2014. Characterization and Beneficiation Studies of a Low Grade Bauxite Ore. J. Inst.
767   Eng. Ser. D 95, 81–93. https://doi.org/10.1007/s40033-014-0050-8

768   Reichert, J., Borg, G., 2008. Numerical simulation and a geochemical model of supergene carbonate-
769   hosted non-sulphide zinc deposits. Ore Geol. Rev. 33, 134–151.
770   https://doi.org/10.1016/j.oregeorev.2007.02.006

771   Roberts, D.R., Scheinost, A.C., Sparks, D.L., 2002. Zinc speciation in a smelter-contaminated soil profile
772   using bulk and microspectroscopic techniques. Environ. Sci. Technol. 36, 1742–1750.
773   https://doi.org/10.1021/es015516c

774   Rodriguez Rodriguez, N., Gijsemans, L., Bussé, J., Roosen, J., Önal, M.A.R., Masaguer Torres, V., Manjón
775   Fernández, Á., Jones, P.T., Binnemans, K., 2020. Selective Removal of Zinc from BOF Sludge by
776   Leaching with Mixtures of Ammonia and Ammonium Carbonate. J. Sustain. Metall. 6, 680–690.
777   https://doi.org/10.1007/s40831-020-00305-3

778   Santoro, L., Boni, M., Rollinson, G.K., Mondillo, N., Balassone, P., Clegg, A.M., 2014. Mineralogical
779   characterization of the Hakkari nonsulfide Zn(Pb) deposit (Turkey): The benefits of QEMSCAN®.
780   Miner. Eng. 69, 29–39. https://doi.org/10.1016/j.mineng.2014.07.002

781   Schulz, B., Merker, G., Gutzmer, J., 2019. Automated SEM mineral liberation analysis (MLA) with
782   generically labelled EDX spectra in the mineral processing of rare earth element ores. Minerals 9.
783   https://doi.org/10.3390/min9090527

784   Schulz, B., Sandmann, D., Gilbricht, S., 2020. Sem-based automated mineralogy and its application in
785   geo-and material sciences. Minerals 10, 1–26. https://doi.org/10.3390/min10111004

786   Seyed Ghasemi, S.M., Azizi, A., 2018. Alkaline leaching of lead and zinc by sodium hydroxide: Kinetics
787   modeling. J. Mater. Res. Technol. 7, 118–125. https://doi.org/10.1016/j.jmrt.2017.03.005

788   Shibayama, A., Takasaki, Y., William, T., Yamatodani, A., Higuchi, Y., Sunagawa, S., Ono, E., 2010.
789   Treatment of smelting residue for arsenic removal and recovery of copper using pyro-
790   hydrometallurgical process. J. Hazard. Mater. 181, 1016–1023.
791   https://doi.org/10.1016/j.jhazmat.2010.05.116

792   Swinkels, L.J., Burisch, M., Rossberg, C.M., Oelze, M., Gutzmer, J., Frenzel, M., 2021. Gold and silver
793   deportment in sulfide ores – A case study of the Freiberg epithermal Ag-Pb-Zn district, Germany.
794   Miner. Eng. 174, 107235. https://doi.org/10.1016/j.mineng.2021.107235

795   Taha, Y., Benzaazoua, M., 2020. Editorial for special issue "Towards a sustainable management of mine
796   wastes: Reprocessing, reuse, revalorization, and repository." Minerals 10, 2017–2020.
797   https://doi.org/10.3390/min10010021

798   Tayebi-Khorami, M., Edraki, M., Corder, G., Golev, A., 2019. Re-thinking mining waste through an
799   integrative. Minerals 9(5), 286.

800 Titshall, L.W., Hughes, J.C., Bester, H.C., 2013. Characterisation of alkaline tailings from a lead/zinc mine
801   in South Africa and evaluation of their revegetation potential using five indigenous grass species.
802   South African J. Plant Soil 30, 97–105. https://doi.org/10.1080/02571862.2013.807361

803 Tripathy, S.K., Murthy, Y.R., Singh, V., Farrokhpay, S., Filippov, L.O., 2019. Improving the quality of
804   ferruginous chromite concentrates via physical separation methods. Minerals 9, 10–13.
805   https://doi.org/10.3390/min9110667

806 Tuhý, M., Hrstka, T., Ettler, V., 2020. Automated mineralogy for quantification and partitioning of
807   metal(loid)s in particulates from mining/smelting-polluted soils. Environ. Pollut. 266.
808   https://doi.org/10.1016/j.envpol.2020.115118

809 Vanderbruggen, A., Gugala, E., Blannin, R., Bachmann, K., Serna-Guerrero, R., Rudolph, M., 2021.
810   Automated mineralogy as a novel approach for the compositional and textural characterization of
811   spent lithium-ion batteries. Miner. Eng. 169, 106924.
812   https://doi.org/10.1016/j.mineng.2021.106924

813 Wang, X., Geysen, D., Tinoco, S.V.P., D'Hoker, N., Van Gerven, T., Blanpain, B., 2015. Characterisation of
814   copper slag in view of metal recovery. Trans. Institutions Min. Metall. Sect. C Miner. Process. Extr.
815   Metall. 124, 83–87. https://doi.org/10.1179/1743285515Y.0000000004

816 Warlo, M., Wanhainen, C., Bark, G., Butcher, A.R., McElroy, I., Brising, D., Rollinson, G.K., 2019.
817   Automated quantitative mineralogy optimized for simultaneous detection of (precious/critical)
818   rare metals and base metals in a production-focused environment. Minerals 9.
819   https://doi.org/10.3390/min9070440

820 Xanthopoulos, P., Agatzini-Leonardou, S., Oustadakis, P., Tsakiridis, P.E., 2017. Zinc recovery from
821   purified electric arc furnace dust leach liquors by chemical precipitation. J. Environ. Chem. Eng. 5,
822   3550–3559. https://doi.org/10.1016/j.jece.2017.07.023

823 Xu, C., Zhong, C., Lyu, R., Ruan, Y., Zhang, Z., Chi, R., 2019. Process mineralogy of Weishan rare earth ore
824   by MLA. J. Rare Earths 37, 334–338. https://doi.org/10.1016/j.jre.2018.06.008

825 Zhang, Q., Feng, Q., Wen, S., Cui, C., Liu, J., 2019. A novel technology for separating copper, lead and zinc
826   in flotation concentrate by oxidizing roasting and leaching. Processes 7.
827   https://doi.org/10.3390/PR7060376

828 Zhang, X., Guo, J., Wu, S., Chen, F., Yang, Y., 2020. Divalent heavy metals and uranyl cations incorporated
829   in calcite change its dissolution process. Sci. Rep. 10, 1–15. https://doi.org/10.1038/s41598-020-
830   73555-6

831 Zhao, P., Lu, L., Liu, X., De La Torre, A.G., Cheng, X., 2018. Error analysis and correction for quantitative
832   phase analysis based on rietveld-internal standard method: Whether the minor phases can be
833   ignored? Crystals 8, 1–11. https://doi.org/10.3390/cryst8030110

834

835